Chapter 5

Parameter estimation of coalescing supermassive black hole binaries with LISA

5.1 Introduction to Laser Interferometer Space Antenna

5.1.1 The LISA configuration

Detection of low frequency GWs ($\leq$ 1Hz) is not feasible with the ground based detectors because of seismic noise. Laser Interferometer Space Antenna (in short LISA) is a planned space based GW observatory sensitive to GWs of frequency $10^{-5} - 1$Hz [192, 193]. Typical sources in this frequency band include a wide variety of short period binaries (both galactic and extra galactic), stochastic GW background generated by some physical processes such as inflation in the very early universe, extreme mass ratio inspirals of a stellar mass BH falling into a supermassive BH (SMBH) companion and inspiral and consequent merger of two SMBH binaries which is the topic of discussion of this chapter (See Ref [164] for a review on the science potential of LISA).

LISA is a (equilateral) triangular space craft constellation, whose distance between adjacent arms is 5 million kilometers. This constellation will orbit around the sun with a $20°$ lag w.r.t earth. The constellation will have a tilt of $60°$ with the ecliptic plane which contains the sun and the earth.

LISA, like the ground based detectors, is *not* a 'pointed instrument' but an all-sky monitor with a quadrupolar antenna pattern. The time varying length of the LISA arms, caused by the incident GW signal, is what is measured. With its three arms, one can construct two linearly independent differences. Thus LISA will be able to measure both the polarizations of the incident GW *simultaneously*. For triangulating a source in the sky with the ground

based detectors, one will need a three detector network. LISA, on the other hand, with its orbital motion induced modulations can locate the source without requiring the second interferometer, though the second interferometer improves the estimation.

The orbital motion of LISA induces frequency, phase and amplitude modulations which encode the information about the source's location and orientation. The amplitude modulation is caused by the change in the detector's antenna pattern in the sky due to the orbital motion. Translational motion of the detector towards and away from the source during its orbital motion causes frequency modulation due to Doppler effect. Variation with time of the two antenna pattern functions modulates the phase of the wave. (See [194] for a discussion about these effects and how one can subtract out these effects while analysing the data). The resultant antenna pattern which captures all these modulations is discussed later in the chapter in Sec 5.3.3.

5.1.2   Data analysis for LISA: Time delay interferometry

Maintaining the giant LISA constellation in space is a challenging task for the experimenters. Unlike the ground based detector case, its impossible to bounce the laser beams between different arms because of the large arm lengths involved. Hence Doppler tracking will be employed to track the space crafts with laser beams. One will have six Doppler data streams due to the exchange between three arms.

Phase fluctuations in the master laser causes laser phase noise which is the most important noise source several orders of magnitude larger than the instrumental noise. Cancelling the laser phase noise is an important issue for LISA to achieve the design sensitivity. Since it is impossible to maintain equal arm lengths, the cancellation of laser phase noise is a non-trivial issue.

A strategy to overcome this problem is to combine different data streams with appropriate time delays so as to cancel the laser noise. This is called time delay interferometry (TDI) [25, 26, 27] (See [28] for a review). By properly time shifting the data generated by each readout, one can construct observables which are not only insensitive to the laser phase noise and optical bench motions but also account for different couplings to gravitational radiation and to the other system noises.

In the present work, however, we shall not use the TDI variables. Instead we work with a simplified assumption that noises in the two detectors are uncorrelated.

5.2   Gravitational wave astronomy with LISA

5.2.1   Astrophysical sources for LISA

Most of our near-by galaxies harbour supermassive black holes (BH) at their centre [195]. If this is the case, then merger of such galaxies would produce a binary system composed of two supermassive BHs. Simulations indicate that there could be primordial supermassive BH binaries at the centres of the first galaxies [196]. An understanding of the formation and evolution of these binaries is very important from the view point of cosmology and structure formation. Many of these binaries coalesce under gravitational wave (GW) radiation reaction within Hubble time. Supermassive BH binaries in the mass range 10^4–$10^7 M_\odot$ will emit gravitational waves (GW) of frequency 10^{-4}–10^{-1} Hz during its adiabatic inspiral phase which can be observed by the proposed space-borne GW missions such as LISA [192, 197] with high (~ a few thousands) signal to noise ratio (SNR) up to very high redshifts (~ 10).

Many earlier have investigated the implications of these observations in the context of astrophysics, cosmology and testing general relativity and its alternatives. LISA observations of BH coalescences can be used to study the growth of BHs as the universe evolved and for mapping the distribution of BHs as function of the redshift [198, 21, 199]. LISA will be able to measure luminosity distances to the sources with an accuracy $\sim 1 - 10\%$. If the redshift associated with the event is known by electromagnetic observations, these sources can be used as very high precision standard candles and to study the distance-redshift relation [200, 201]. Ref [202] discussed the potential of LISA to observe binaries containing a BH in the intermediate mass regime ($\sim 10^3 M_\odot$) and use it as a probe of strong field aspects of gravity.

5.2.2   Test of strong-field gravity using LISA

LISA could probe many strong gravitational field effects which are not possible to explore with other observational means. Both inspiral and ring-down GW signals can be used for this. Refs [203, 204, 24] studied the possibility of using the quasi-normal mode oscillations to test the no-hair theorem of general relativity since these modes will be characterized *only* by the mass and angular momentum of the BH (in general relativity). Hughes and Menou examined another possibility [205] assuming LISA detects both inspiral and ring-down signals from the same source. By measuring the total mass independently from both the inspiral and ringdown signals one can estimate the mass difference which will be the mass-energy lost due to GWs. They suggested that an extension of this idea including spin effects could in principle test the BH area theorem. Further, inspiral of a stellar mass BH into a SMBH will be another interesting source for LISA using which many properties of the central SMBH can be probed including the possibility to map the spacetime by following the geodesic mo-

tion of the stellar mass BH (See e.g.[206, 207]) and measuring the multipole moments of the spacetime.

LISA will provide an unique opportunity to test general relativity and its alternatives. Will and his co-workers have discussed the potential of LISA to test general relativity as well as its alternatives like Brans-Dicke theory and massive graviton theories [208, 209]. Recently this issue was discussed in a more realistic scenario of spinning binaries using 2PN phasing [21, 199]. Blanchet and Sathyaprakash proposed another test based on the post-Newtonian (PN) GW phasing formula by measuring the 1.5PN GW tail effect and showing how it can be used as a test of general relativity [186, 187]. This proposal was recently generalized to higher PN order terms in the phasing formula in Refs [190, 22, 23] and it was argued that such a test would allow one to probe the nonlinear structure of gravity.

5.2.3   Parameter estimation problem in the LISA context

A very accurate parameter extraction scheme is central to performing all these analyses. A parameter estimation scheme based on matched filtering, similar to that for the ground based detectors such as LIGO and VIRGO, will be employed for LISA also. An efficient matched filtering would in turn demand a very accurate model of the gravitational waveform. In order to compute the gravitational waveform from a compact binary system, one solves the two-body problem in general relativity perturbatively using different approximation schemes since no exact solutions for this problem exist till date. The final waveform can be expressed as a post-Newtonian expansion which is a power series in v/c where v is the gauge independent velocity parameter characterising the source (See Ref. [44] for an exhaustive review on the formalism). In our notation $\frac{v}{c}$ refers to half a PN order.

Since the information about the phase is more important for the process of matched filtering, one uses a simplified model of the inspiral waveform (the so called restricted waveform) where phase is modelled to a high PN order but retaining only the Newtonian amplitude. In doing so, one is neglecting the effect of other harmonics [101, 102] in the waveform and also the higher order PN corrections to the dominant harmonic at twice the orbital frequency. In the present study, we deal only with the restricted waveform in the Fourier domain obtained using stationary phase approximation. The phasing formula for nonspinning binaries, is presently complete up to 3.5PN order [97, 99, 100]. In the case of spinning binaries, the phasing formula with all spin effects (spin-orbit and spin-spin interactions) included is available to 2PN order [117, 118]. Recently the 2.5PN phasing formula with spin-orbit coupling was obtained in Refs [119, 160]. We discuss its possible implications for parameter estimation in the concluding section.

The implications of the higher PN order phasing in the context of parameter estima-

tion problem has been investigated by different authors. Based on the framework set up by Refs [184, 185], Cutler and Flanagan [103] investigated the importance of the 1.5PN phasing formula [96]. The effect of including the spin-orbit coupling parameter at 1.5PN order into the space of parameters was one of interesting issues addressed. Next, two independent works by Krolak *et al.* [104] and Poisson and Will [105] analysed the problem of parameter estimation using the 2PN phasing formula of Ref. [97]. Inclusion of the 2PN spin-spin coupling term at 2PN and its effect on estimation of the other parameters was the focus of their analysis.

The work discussed in the previous chapter investigated the effect of the 2.5, 3 and 3.5PN terms for the parameter estimation of nonspinning binaries in the LIGO and VIRGO cases (a similar work was carried out independently by Berti and Buonanno [210]). Using the covariance matrix calculations, they inferred that by employing the 3.5PN phasing instead of the 2PN one, the estimation of chirp mass and symmetric mass ratio improves by 19% and 52% respectively for the ground based detectors such as LIGO and VIRGO.

Cutler was the first to address the problem of parameter estimation in the LISA context [193]. He used the 1.5PN waveform including the spin-orbit effect and studied the estimation of errors associated with the mass parameters as well as distance and angular resolution of the binary. Seto investigated the effect of finite arm length of LISA using 1.5PN phasing [211]. Vecchio revisited the parameter estimation with the 1.5PN waveform [212] where he used the waveform for circular orbit but with "simple precession" (as opposed to non-precessing case of [193]) and examined the implications of it for the estimation of distance and angular resolution. Various aspects of the 2PN parameter estimation, such as the spin-spin coupling, was investigated by different authors [198, 21, 199]. Ref [21] studied the effect of spin terms in testing alternate theories of gravity with the LISA observations. Refs [198, 199] also addressed the issue of mapping the merger history of massive BHs using LISA observations with the 2PN phasing. While all these calculations are within the restricted waveform approximation where the PN corrections to the amplitude is completely neglected, there are investigations about the effect of including these amplitude corrections in the context of parameter estimation [123, 124, 121, 122].

Other than the covariance matrix approach, which is valid only in the high SNR limit, there have been proposals in literature addressing the parameter estimation problem using Monte-Carlo methods. In Ref [173], the authors compared the error estimates obtained using the covariance matrix with the Monte-Carlo simulations. Recently parameter estimation schemes based on Bayesian statistics using Markov chain Monte-Carlo (MCMC) method also has been proposed and implemented in the ground based detector context [213, 214] and the LISA case [215, 216]. Using the 2PN waveform Ref [215] found that posterior parameter estimation distribution of the *extrinsic parameters* obtained using MCMC methods are in

excellent agreement with those computed using Fisher matrix whereas there is a systematic overestimate of the errors by Fisher matrix for the *intrinsic parameters*.

In the present work we extend the earlier analyses to the observation of GW inspirals of supermassive BH binaries by LISA. Coalescences of BHs of masses $10^4 - 10^7 \, M_\odot$ at a luminosity distance of 3 Gpc are considered. We assume LISA will observe these events for one year duration. Using the 3.5PN phasing we calculate the errors associated with the estimation of the mass parameters, distance and angular resolution and compare them to the corresponding 2PN results. We also study the effect of orbital motion on parameter estimation by comparing these results with other two cases, one where LISA pattern functions are not used and another when LISA is considered to be a two detector network instead of a single Michelson interferometer.

The rest of the chapter is organized as follows. Sec. 5.3 discusses all the necessary inputs required for the chapter such as a brief introduction to parameter estimation using covariance matrix, noise model for LISA, model for the waveform and some other conventions followed in the chapter. Secs 5.4 and 5.5 discuss the main results and their implications and Sec. 5.6 contain a summary and finally Sec 5.7 the future directions.

5.3 The 3.5PN parameter estimation for LISA: Models and assumptions

5.3.1 Parameter estimation using the covariance matrix

We summarize the theory of parameter estimation in the context of Gaussian random detector noise, addressed in the GW context first by Finn and Chernoff [184, 185] and implemented by Cutler and Flanagan [103]. Let us assume an inspiral GW signal is detected meeting the necessary detection criteria and that one needs to extract the intrinsic and extrinsic parameters from the signal by matched filtering. In the next paragraph, we briefly summarize the parameter estimation theory explained in detail in chapter 4

For sources like inspiralling compact binaries, where a prior source modelling is possible to predict the gravitational waveform, *matched filtering* is an ideal method both for detection as well as parameter estimation of the signal [166]. In matched filtering, the detector output is filtered using a bank of theoretical templates with different signal parameters. The parameters of the template which obtains the best signal-to-noise ratio (SNR) gives the "measured" values of the signal parameters. These values, in general, will be different from the "actual" values due to the presence of noise. The problem of parameter estimation addresses the question of how close are the measured values to the actual ones and what the associated errors are in the estimation of different parameters. For a given signal, different realizations of

noise lead to different sets of best-fit parameters of the signal. When the background noise is a stationary, random, Gaussian process, at high enough SNRs the best-fit values of the parameters have a Gaussian distribution centered around the actual values of the parameters.

If λ^i denotes the actual value of the parameters and $\lambda^i + \Delta\lambda^i$, the measured value, then the root mean square difference $\Delta\lambda^i$ obeys a Gaussian distribution: $p(\Delta\lambda_i) \propto \exp\left(-\Gamma_{ij}\Delta\lambda^i\Delta\lambda^j/2\right)$ where Γ_{ij}, the Fisher information matrix constructed from the Fourier domain representation of the waveform, is given by

$$\Gamma_{ij} = 2 \int_{f_{in}}^{f_{fin}} \frac{\tilde{h}_i^*(f)\tilde{h}_j(f) + \tilde{h}_i(f)\tilde{h}_j^*(f)}{S_h(f)} \, df. \tag{5.1}$$

Here, $\tilde{h}_i(f) := \partial\tilde{h}(f)/\partial\lambda^i$, $\tilde{h}(f)$ is the Fourier domain gravitational waveform and $S_h(f)$ is the (one-sided) noise power spectral density of the detector. It also follows that the root-mean-square error in measuring λ^i is given by $\sigma^i = \sqrt{\Sigma^{ii}}$, where $\Sigma = \Gamma^{-1}$ is called the *covariance matrix*. The non-diagonal elements of the covariance matrix define the correlation coefficient between two parameters: $c^{ij} := \frac{\Sigma^{ij}}{\sqrt{\Sigma^{ii}\Sigma^{jj}}}$. Repeated indices are *not* summed over in the above expressions. Finally, the SNR ρ can be expressed in terms of the Fourier domain signal $\tilde{h}(f)$ as

$$\rho^2 = 4 \int_{f_{in}}^{f_{fin}} \frac{|\tilde{h}(f)|^2}{S_h(f)} \, df. \tag{5.2}$$

In the present case of LISA the λ^i denoting the set of our chosen parameters are given by $\{t_c, \phi_c, \mathcal{M}, \eta, D_L, \bar{\phi}_S, \bar{\phi}_L, \bar{\theta}_S, \bar{\theta}_L\}$. In the case where pattern functions are not included the above set reduces to $\{t_c, \phi_c, \mathcal{M}, \eta\}$. The additional elements of the parameter set denote the distance, orientations and locations of the source in the sky specified with respect to the fixed solar system based coordinate system.

In the above integrals, the upper limit of integration is $f_{fin} = \text{Min}[f_{lso}, f_{end}]$, where f_{lso} is the frequency of the innermost stable circular orbit for the test particle case, $f_{lso} = (6^{3/2}\pi m)^{-1}$ and f_{upper} corresponds to the upper cut-off of the LISA noise curve $f_{end} = 1\text{Hz}$. We have chosen the lower limit of frequency $f_{in} = \text{Max}[f_{in}, f_{lower}]$ where f_{in} is calculated by assuming the signal lasts for one year in the LISA sensitivity band and f_{lower}, the low frequency cut-off for LISA noise curve, is assumed to be 10^{-5}Hz[1].

5.3.2 Model for the LISA noise curve

We follow the noise model of LISA as given in Ref [21] which is a slightly modified version of [217]. The noise spectral density consists of a non-sky averaged part [217] and confusion

---

[1]Another way of choosing the limits of integration is to calculate the time over which the signal will last once it enters the LISA band. See [198] for example, where the duration of the signal is calculated using the expression for $t(f)$. It assumes $f_{lower} = 10^{-4}\text{Hz}$ and 3 year mission time for LISA.

noise due to the galactic and extra-galactic white dwarf binaries [218, 219, 217]. The total instrumental plus confusion noise reads as

$$S_h(f) = \min\left\{\frac{S_h^{\text{NSA}}(f)}{\exp\left(-\kappa T_{\text{mission}}^{-1} dN/df\right)}, S_h^{\text{NSA}}(f) + S_h^{\text{gal}}(f)\right\} + S_h^{\text{ex-gal}}(f), \qquad (5.3)$$

where $S_h^{\text{NSA}}(f)$ refers to the non-sky averaged part of spectral density. The noise contributions from the galactic and extra-galactic white-dwarf binaries are represented by $S_h^{\text{gal}}(f)$ and $S_h^{\text{ex-gal}}(f)$, respectively, and dN/df refers to the number density of galactic white-dwarf binaries per unit GW frequency. The corresponding expressions are given by

$$\begin{aligned}
S_h^{\text{NSA}}(f) &= \left[9.18 \times 10^{-52}\left(\frac{f}{1\,\text{Hz}}\right)^{-4} + 1.59 \times 10^{-41}\right. \\
&\quad \left. + 9.18 \times 10^{-38}\left(\frac{f}{1\,\text{Hz}}\right)^{2}\right]\,\text{Hz}^{-1}, & (5.4a)
\end{aligned}$$

$$S_h^{\text{gal}}(f) = 2.1 \times 10^{-45}\left(\frac{f}{1\,\text{Hz}}\right)^{-7/3}\,\text{Hz}^{-1}, \qquad (5.4b)$$

$$S_h^{\text{ex-gal}}(f) = 4.2 \times 10^{-47}\left(\frac{f}{1\,\text{Hz}}\right)^{-7/3}\,\text{Hz}^{-1}, \qquad (5.4c)$$

$$\frac{dN}{df} = 2 \times 10^{-3}\,\text{Hz}^{-1}\left(\frac{1\,\text{Hz}}{f}\right)^{11/3}, \qquad (5.4d)$$

where T_{mission} is the duration of LISA mission. See Sec II C of Ref [21] for a detailed summary.

5.3.3 The waveform model

LISA with its three arms is essentially equivalent to a pair of two-arm detectors. We consider two cases: one where we assume the estimation of mass parameters is not affected because of their correlations with the angular variables and second when we estimate the associated errors with angular variables and luminosity distance of the source. Since the information about the angular variables are encoded in the so-called pattern functions which describes the orbital motion of LISA, in the first case we use a waveform which is averaged over the pattern functions. In the second case, we do not average over the pattern functions and use the information from the LISA orbital motion to discuss the estimation of angular resolution and luminosity distance to the source. Further, in the second case we consider cases when (i) LISA is a single two arm-detector and (ii) as a two detector network in order to understand the effect of network configuration for parameter estimation. The LISA antenna patterns, describing its orbital motion, is given in [193] which is used for the present study (also see

Appendix A of Ref [21] for these expressions).

Unlike the ground based detectors where the two arms have an angle 90°, the LISA arms are at 60°. As shown by Cutler [193], the relative strain amplitude in the LISA case can be simply related to the 90° interferometer case by multiplying the latter by a factor $\sqrt{3}/2$. Using this input, the Fourier domain waveform within the stationary phase approximation can be written down as [193, 21]

$$\tilde{h}_\alpha(f) \;=\; \frac{\sqrt{3}}{2} \mathcal{A} f^{-7/6} e^{i\psi(f)}, \qquad \alpha = \mathrm{I, II}, \tag{5.5a}$$

$$\mathcal{A} \;=\; \frac{1}{\sqrt{30}\pi^{2/3}} \frac{\mathcal{M}^{5/6}}{D_{\mathrm{L}}}, \tag{5.5b}$$

where α labels the interferometer, f the GW frequency and $\mathcal{M}$, the chirp mass which is related to total mass $m = m_1 + m_2$ and symmetric mass ratio $\eta = m_1 m_2/m^2$ by $\mathcal{M} = \eta^{3/5} m$. The luminosity distance to the source is denoted by D_L. The GW phase $\psi(f)$ appearing in the formula is completed up to 3.5PN [100, 99, 143] and its Fourier domain representation is given in [47, 106]. We find it more convenient to write it as

$$\psi(f) = 2\pi f\, t_c - \phi_c + \sum_{k=0}^{k=7} \alpha_k\, v^k, \tag{5.6}$$

where $v = (\pi m f)^{1/3}$ is the PN variable which is related to gauge independent source velocity in system of units where $G = 1 = c$ which we follow henceforth in the chapter. Eq (4.18) of chapter 4 gives the α_k for different values of $k = 0 \cdots 7$.

In the case where we do not average the pattern functions, the waveform can be written as [21]

$$\tilde{h}_\alpha(f) = \frac{\sqrt{3}}{2} \mathcal{A} f^{-7/6} e^{i\Psi(f)} \left\{ \frac{5}{4} \tilde{A}_\alpha(t(f)) \right\} e^{-i\left(\varphi_{p,\alpha}(t(f)) + \varphi_D(t(f))\right)}, \tag{5.7}$$

where $\varphi_{p,\alpha}(t(f))$ and $\varphi_D(t(f)$ are the polarization phase and Doppler phase respectively [193]. $\tilde{A}_\alpha(t(f))$ correspond to the amplitude modulations induced by the LISA's orbital motion. $\tilde{A}_\alpha(t(f))$ and $\varphi_{p,\alpha}(t(f))$ depends on the pattern functions $F_+^\alpha(t)$ and $F_\times^\alpha(t)$ and hence vary with time. For convenience, all the essential equations related to the response of LISA [193, 21] are given below.

In the equations below, 'barred' quantities are in the fixed-solar system based coordinate systems and those 'unbarred' are in the rotating LISA frame. We assume that noise is symmetric in each pair of the LISA arms and hence treat LISA to be consisting of two independent Michelson interferometers in the shape of an equilateral triangle. Compared to the ground based detector case, the resultant waveform will have an overall $\frac{\sqrt{3}}{2}$ factor to account

for the equilateral geometry [193]. The pattern functions are given by

$$
\begin{aligned}
F_{\mathrm{I}}^{+}(\theta_S,\phi_S,\psi_S) &= \frac{1}{2}(1+\cos^2\theta_S)\cos 2\phi_S \cos 2\psi_S \\
&\quad - \cos\theta_S \sin 2\phi_S \sin 2\psi_S \ , \\
F_{\mathrm{I}}^{\times}(\theta_S,\phi_S,\psi_S) &= \frac{1}{2}(1+\cos^2\theta_S)\cos 2\phi_S \sin 2\psi_S \\
&\quad + \cos\theta_S \sin 2\phi_S \cos 2\psi_S \ ,
\end{aligned}
\tag{5.8}
$$

and

$$
\begin{aligned}
F_{\mathrm{II}}^{+}(\theta_S,\phi_S,\psi_S) &= F_{\mathrm{I}}^{+}\left(\theta_S,\phi_S - \frac{\pi}{4},\psi_S\right), \\
F_{\mathrm{II}}^{\times}(\theta_S,\phi_S,\psi_S) &= F_{\mathrm{I}}^{+}\left(\theta_S,\phi_S - \frac{\pi}{4},\psi_S\right).
\end{aligned}
\tag{5.9}
$$

In the above equations we have denoted by (θ_S,ϕ_S) the source location and by ψ_S the polarization angle defined as

$$
\tan\psi_S(t) = \frac{\hat{\mathbf{L}}\cdot\mathbf{z} - (\hat{\mathbf{L}}\cdot\mathbf{n})(\mathbf{z}\cdot\mathbf{n})}{\mathbf{n}\cdot(\hat{\mathbf{L}}\times\mathbf{z})} \ ,
\tag{5.10}
$$

$\hat{\mathbf{L}}$, $\mathbf{z}$ and $-\mathbf{n}$ being the unit vectors along the orbital angular momentum, the unit normal to *LISA*'s plane and the GW direction of propagation, respectively.

The waveform polarization and Doppler phases in the above equations are given by :

$$
\varphi_{p,\alpha}(t) = \tan^{-1}\left[\frac{2(\hat{\mathbf{L}}\cdot\mathbf{n})F_{\alpha}^{\times}(t)}{(1+(\hat{\mathbf{L}}\cdot\mathbf{n})^2)F_{\alpha}^{+}(t)}\right] \ ,
\tag{5.11a}
$$

$$
\varphi_D(t) = \frac{2\pi f}{c}R\sin\bar{\theta}_S\,\cos(\bar{\phi}(t)-\bar{\phi}_S) \ ,
\tag{5.11b}
$$

where $\alpha = \mathrm{I},\mathrm{II}$, with $R = 1$ AU and $\bar{\phi}(t) = \bar{\phi}_0 + 2\pi t/T$. Here $T = 1$ year is the orbital period of *LISA*, and $\bar{\phi}_0$ is a constant that specifies the detector's location at time $t = 0$. Since we consider nonprecessing binaries $\hat{L}^a$ points in a fixed direction $(\bar{\theta}_L,\bar{\phi}_L)$.

To express the angles (θ_S,ϕ_S,ψ_S) evaluated with respect to the rotating detector-based coordinate system as function of the angles $(\bar{\theta}_S,\bar{\phi}_S,\bar{\theta}_L,\bar{\phi}_L)$ evaluated with respect to the fixed solar-system based coordinate system, we use the following relations [193]:

$$
\cos\theta_S(t) = \frac{1}{2}\cos\bar{\theta}_S - \frac{\sqrt{3}}{2}\sin\bar{\theta}_S \cos(\bar{\phi}(t)-\bar{\phi}_S) \ ,
\tag{5.12a}
$$

$$
\phi_S(t) = \alpha_0 + \frac{2\pi t}{T} + \tan^{-1}\left[\frac{\sqrt{3}\cos\bar{\theta}_S + \sin\bar{\theta}_S \cos(\bar{\phi}(t)-\bar{\phi}_S)}{2\sin\bar{\theta}_S \sin(\bar{\phi}(t)-\bar{\phi}_S)}\right] ,
\tag{5.12b}
$$

where α_0 is a constant specifying the orientation of the arms at $t = 0$. We take $\alpha_0 = 0$ and $\bar{\phi}_0 = 0$, corresponding to a specific choice of the initial position and orientation of the

detector [193]. Also,

$$\mathbf{z} \cdot \mathbf{n} = \cos \theta_S \,, \tag{5.13a}$$

$$\hat{\mathbf{L}} \cdot \mathbf{z} = \frac{1}{2}\cos \bar{\theta}_L - \frac{\sqrt{3}}{2}\sin \bar{\theta}_L \cos \left(\bar{\phi}(t) - \bar{\phi}_L\right) \,, \tag{5.13b}$$

$$\hat{\mathbf{L}} \cdot \mathbf{n} = \cos \bar{\theta}_L \cos \bar{\theta}_S + \sin \bar{\theta}_L \sin \bar{\theta}_S \cos \left(\bar{\phi}_L - \bar{\phi}_S\right) \,, \tag{5.13c}$$

$$\mathbf{n} \cdot (\hat{\mathbf{L}} \times \mathbf{z}) = \frac{1}{2}\sin \bar{\theta}_L \sin \bar{\theta}_S \sin \left(\bar{\phi}_L - \bar{\phi}_S\right)$$

$$-\frac{\sqrt{3}}{2}\cos\bar{\phi}(t)\Big(\cos \bar{\theta}_L \sin \bar{\theta}_S \sin \bar{\phi}_S - \cos \bar{\theta}_S \sin \bar{\theta}_L \sin \bar{\phi}_L\Big)$$

$$-\frac{\sqrt{3}}{2}\sin\bar{\phi}(t)\Big(\cos \bar{\theta}_S \sin \bar{\theta}_L \cos \bar{\phi}_L - \cos \bar{\theta}_L \sin \bar{\theta}_S \cos \bar{\phi}_S\Big) \,. \tag{5.13d}$$

For 3.5PN accurate expression for $t(f)$ in Eq (5.7) we use the following relation

$$2\pi\, t(f) = \frac{d\,\psi(f)}{df}. \tag{5.14}$$

This can be rewritten as

$$t(f) = t_c - \sum_{k=0}^{7} t_k^v v^k, \tag{5.15}$$

and values of t_k^v is given in Refs [47, 106] which can readily be used.

For calculations where LISA is assumed to be a two detector network, we calculate the SNR and Fisher matrix using

$$\rho^{\text{Network}} = \sqrt{\rho_{\text{I}}^2 + \rho_{\text{II}}^2}, \tag{5.16}$$

$$\Gamma_{ab}^{\text{Network}} = \Gamma_{ab}^{\text{I}} + \Gamma_{ab}^{\text{II}}. \tag{5.17}$$

The errors for the two detector case are obtained inverting the total Fisher matrix following the procedure outlined in Sec. 5.3.1.

Throughout the chapter we assume a cosmological model with zero spatial curvature $\Omega_\kappa = 0$ and $\Omega_\Lambda + \Omega_M = 1$, where Ω_M and Ω_Λ refers to the contributions to the total density from matter and cosmological constant. Hubble's constant is assumed to be $H_0 = 70$ km s^{-1} Mpc^{-1}. The luminosity distance is given by

$$D_L = \frac{1 + z}{H_0} \int_0^z \frac{dz'}{[\Omega_M(1 + z')^3 + \Omega_\Lambda]^{1/2}} \,, \tag{5.18}$$

where z denotes the redshift of the source.

We calculate the Fisher matrix for the different configurations of LISA using the cor-

responding waveforms and invert it to get the covariance matrix. The elements of the covariance matrix are used for discussing the errors and correlation coefficients of different parameters in the next section. While discussing the trends with the PN orders, its useful to keep in mind that apart from the usual phase $\psi(f)$, there are additional PN series of $t(f)$ both in the amplitude and phase when pattern functions are included, which can influence the results.

5.4 Parameter estimation with pattern averaged waveform

In this section we discuss the parameter estimation in the LISA case using pattern averaged waveform of Eq (5.5b). Parameter estimation with the non-pattern averaged waveform (as in Eq 5.7) is more complex since the estimated errors strongly depend on the *location and orientation* of the source (see the Sec. 5.5 below) which enter the calculation via the pattern functions. The ideal way to deal with the situation will be to perform Monte Carlo simulations for different binaries located and oriented randomly in the sky [198, 212, 21, 199]. A recent work [21] (which addressed the parameter estimation problem using the 2PN waveform including spin effects) compared the results of a Monte Carlo simulation with the result obtained using pattern averaged waveform (see Tables V, VI and VIII of Ref [21]). It found that the results in both the cases are in excellent agreement. The results presented in this section about the improved parameter estimation with the pattern averaged waveform, may hence give a reasonably good idea about the full problem where the LISA pattern functions are included and it is considered to be a two detector network. We emphasize that the results quoted here have to be supported by Monte Carlo simulations similar to Ref [21] (see concluding remarks in Sec. 5.6).

5.4.1 Improved parameter estimation of equal mass binaries with the 3.5PN phasing

We discuss the performance of the 3.5PN restricted waveform from the parameter estimation point of view for the pattern-averaged case discussed above. Our aim is to study the variation of errors in different parameters with the total observed mass[2] of the binary for different PN orders. This would not only give us an idea of the improvement brought in by the use of higher order phasing but also about the convergence of the PN series for the problem of parameter estimation. We have checked our codes by reproducing the results at 2PN with that in Table III and V of Ref [21] for the nonspinning case. The important results of our

---

[2]By total mass, we always refer to the total redshifted mass $m'(1 + z)$, where m' is the actual source mass and z is the redshift of the source. This is the mass that is observed by the GW observations.
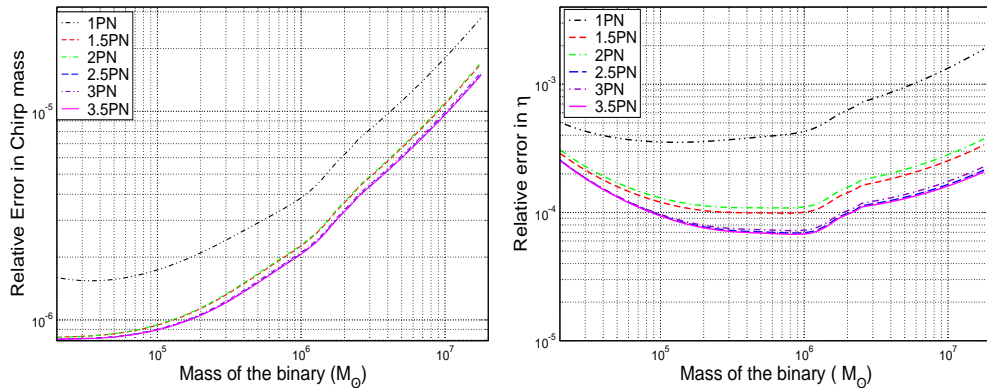
Figure 5.1: Variation of errors with the total observed mass for different PN order restricted waveforms for LISA. The *pattern averaged* waveform is used. The convergence of the results is evident in both the cases. Sources are assumed to be at 3 Gpc.

study are discussed in detail in what follows. The errors in estimation of different parameters for a $2 \times 10^6 M_\odot$ binary at 3 Gpc is provided in Table I for different PN orders in the phasing.

5.4.2 Improvement in estimation of mass parameters and the PN convergence

Improvement due to higher order terms: We plot in Fig. 5.1 the variation with mass of the errors in chirp mass and η for different PN orders. There is significant improvement in the estimation by the use of the 3.5PN phasing instead of the 2PN one especially for more massive systems. For a prototypical system of a binary BH each of mass $10^6 M_\odot$, we find that the chirp mass and η improve by 11% and 39% respectively. Improvement is higher for more massive systems. For a $2 \times 10^7 M_\odot$ binary, the chirp mass and η improves by 14% and 45%. They are similar to the results for the ground based detectors as discussed in [220] but in an entirely different mass range. For a typical binary in its sensitivity band, LISA will be able to measure chirp mass with an incredibly small fractional accuracy of $\sim 10^{-6}$ and η by about $\sim 10^{-4}$.

Variation with mass: The estimation of the chirp mass worsens with increase in total mass of the binary whereas the estimation of η improves initially and then decreases. These effects can be understood as follows. When the total mass increases there are two competing effects in action: the increase in errors with mass, since signal lasts for smaller duration, and the variation of SNR with mass, which is a characteristic of the noise curve. For chirp mass the errors increase so rapidly that the variation in SNR does not affect the trend and the errors continue to increase monotonically with mass. For η, there is trade-off between these two competing effects which accounts for the minima in the curve.
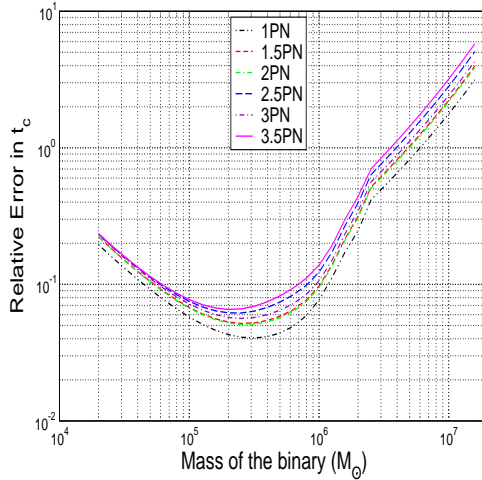
Figure 5.2: Variation of errors in t_c with the total observed mass for different PN order restricted waveforms for LISA. The *pattern averaged* waveform is used. The convergence of the results is evident from the plot. Sources are assumed to be at 3 Gpc.

5.4.3 Errors in coalescence time

Measuring the time of coalescence of a binary system is important to carry out electromagnetic observation of the event associated with the binary merger. We discuss the trends in the estimation of t_c below.

Fig. 5.2 displays the variation of errors in t_c with increasing mass of the source and across the PN orders. The errors in t_c show trends similar to that of [220], *i.e.,* with increase in PN order the errors oscillate in a sense opposite to the mass parameters and in going from 2PN to 3.5PN there is a net degradation in its estimation, which is about 43% for the $2 \times 10^6 M_\odot$ system considered. This was explained in chapter 4 based on the correlations between t_c, $\mathcal{M}$ and η. It was noticed that *both* $c_{\mathcal{M}t_c}$ and $c_{\eta t_c}$ are positive and follow the same trend as the error in t_c. Increase in these correlations implied a worsened estimation of t_c.

5.4.4 Post-Newtonian convergence in the parameter estimation context

Since the PN series is an asymptotic series, the rate of convergence of the results is a very important issue for detection as well as parameter estimation. We use the word 'convergence' to mean that the difference (in errors) between two consecutive PN orders is smaller as we go to higher PN orders. As remarked in Refs. [103, 105], if the parameter estimation scheme is based on a lower order (2PN) phasing, the systematic errors due to the absence of higher order terms may be more than the statistical errors caused by the noise. Since we study here the implications of 3.5PN phasing, we examine the convergence of the series based on our results for different PN orders.

As Fig. 5.1 reveals, though there will be improvement by using the 3.5PN phasing instead

Table 5.1: Variation of errors in different parameters and number of GW cycles with PN order. Errors are calculated with the pattern averaged waveform. The system considered is a binary of mass $2 \times 10^6 M_\odot$ at a luminosity distance of 3 Gpc. Most of the features regarding the improvement in parameter estimation, convergence of the PN series and correlation with number of GW cycles are captured in this table.

PN Order	Δt_c (sec)	$\Delta \mathcal{M}/\mathcal{M}$ (10^{-6})	$\Delta \eta/\eta$ (10^{-4})	N_{cycles}
1PN	0.2474	6.217	6.287	2414.03
1.5PN	0.3149	3.648	1.427	2310.26
2PN	0.3074	3.694	1.572	2305.52
2.5PN	0.3947	3.320	0.9882	2314.48
3PN	0.3435	3.377	1.033	2308.73
3.5PN	0.4399	3.300	0.9661	2308.13

of the 2PN one, most of the improvement seems to come from the transition between 2PN and 2.5PN after which the series continues to show its characteristic oscillatory behaviour, but with smaller amplitude, suggesting that phasing at orders higher than 3.5PN may not cause much improvement (see Table I).

5.4.5 Parameter estimation and Number of GW cycles

In Ref. [220], the correlation between the improvement in errors across different PN orders and the number of total and useful GW cycles [46] was studied. It was found that though they are good indicators of how the errors at each order vary with the total mass of the system, they alone cannot explain the variation of errors across different PN orders in the context of ground based detectors. We confirm this feature in the LISA context. We recover the results in Table I and II of Ref [21] as a check of our calculation. Table 5.1 shows how the errors and total GW cycles vary with increasing PN orders. One would expect an improved (worsened) estimation if number of GW cycles increases (decreases) between two consecutive PN orders if they were solely responsible for the trends. From the table it is clear that from 1PN to 1.5PN and 1.5PN to 2PN, the errors in chirp mass and η do *not* conform to the above expectation. The same is the case in going from 3PN to 3.5PN. Finally, trends in t_c being opposite to that of the other two mass parameters lead one to conclude once again that the number of GW cycles is not sufficient to understand the variation of errors across different PN orders.

Irrespective of whether the total number of GW cycles is very high ($\sim 10^5$)(as in the case of LISA) or low ($\sim$ hundreds) (as for the ground based detectors) the PN trends in parameter estimation are too complicated to be explained solely in terms of this. The number of GW

cycles and change in SNR with mass can account for the variation of errors in chirp mass and η with the total mass of the binary.

5.4.6 Parameter estimation for unequal mass binaries

Lastly we perform a similar analysis for unequal mass systems where $\eta < 0.25$. For larger mass ratios ($\eta \simeq 10^{-5}$ or smaller in our case), the Fisher matrix becomes ill-conditioned [21] and hence we restrict ourselves to the inspiral of a binary consisting of an intermediate mass BH (IMBH) and a SMBH rather than stellar mass-SMBH inspirals. An IMBH of $10^4 M_\odot$ inspiralling into a SMBH of $10^6 M_\odot$ constitutes our prototypical system. This system at a distance of 3 Gpc will have a SNR of a few hundreds. We find that the improvement due to the inclusion of higher order terms is more dominant here than for the equal mass binary case. For the prototypical system considered above, we find an improvement of 11% for the chirp mass and 52% for η in the pattern-averaged case. For a $10^4 - 10^7 M_\odot$ binary, where SNR is $\simeq 100$, the improvement is even more: 20% and 62% respectively [3]. Our calculations do not apply to the extreme mass ratio case of, say, $10 M_\odot - 10^6 M_\odot$. This is because the Fisher matrix obtained in this case is very much ill-conditioned.

This larger improvement for the unequal mass binaries is not a special feature of the LISA noise curve; for the ground based detectors also a similar feature exists. But unlike in the LISA case, where many such unequal mass binaries are astrophysically plausible, for the ground based detectors such sources are not prototypical.

5.4.7 Effect of low frequency cut-off chosen

All the calculations so far, and hence the results, have been based on the optimistic possibility that the low frequency sensitivity of LISA can be extrapolated from 10^{-4} Hz to 10^{-5} Hz. As argued in Ref [21], this significantly improves the parameter estimation. We quantify the effect of this choice of lower cut-off by comparing our previous results with the one where LISA is assumed to be 'blind' below 10^{-4}Hz.

As discussed in Sec. 5.3.1, we have chosen the lower limit of integration in all the calculations assuming that the system is observed for one year before coalescence, when $f = f_{\text{lso}}$. By this procedure, the lower cut-off for a $2 \times 10^{5.5} M_\odot$ binary is about 10^{-4} Hz. This means for systems with masses higher than $2 \times 10^{5.5} M_\odot$ (and hence a lower f_{lso}) the lower limit of integration for one year observation time will be less than 10^{-4} Hz. If we assume LISA is not sensitive to signals below 10^{-4} Hz, these systems will be observed effectively for less

---

[3]Using a calculation of the number of GW cycles, Ref [221] has emphasized the need for higher order PN modelling of the IMBH-SMBH binaries. The effects of eccentricity could also play an important role in the dynamics of such binaries.
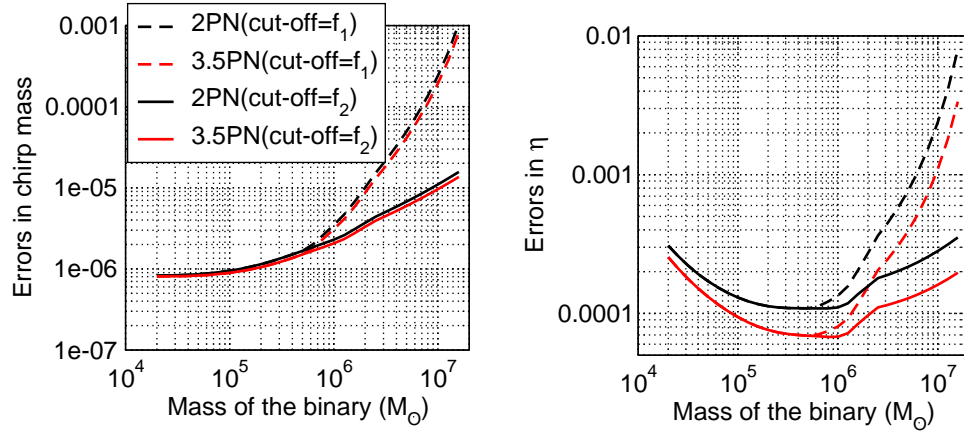
Figure 5.3: The variation with PN order of errors of chirp mass and η with the total observed mass for different PN order restricted waveforms for LISA the lower frequency cut-offs $f_1 = 10^{-4}$ Hz and $f_2 = 10^{-5}$. The *pattern averaged* waveform is used. The sources are assumed to be at 3 Gpc.

than a year leading to a significant decrease in the number of GW cycles and consequent degradation in parameter estimation (for a $2 \times 10^6 M_\odot$ binary, a lower cut-off of 10^{-5} Hz will give 2308 GW cycles as opposed to 608 if the cut-off was 10^{-4} Hz). Thus for binaries whose masses are higher than $2 \times 10^{5.5} M_\odot$, the choice of lower cut-off frequency will affect the results reported here. Fig. 5.3 displays the variation of 2PN and 3.5PN errors in chirp mass and η corresponding to the two different lower frequency cut-offs we have chosen. Indeed, as is evident from the plot, the errors start to deviate for binaries whose masses are greater than $2 \times 10^{5.5} M_\odot$. For a $2 \times 10^7 M_\odot$ system, using 10^{-5} Hz as cut-off instead of 10^{-4} Hz improves the estimation of chirp mass by about 150 times and that of η by 40 times. These results confirm the need to push to the extent possible the lower frequency sensitivity of LISA.

Regarding the improvement in parameter estimation in going from 2PN to 3.5PN, calculation with a cut-off of 10^{-4} Hz shows that for a $2 \times 10^7 M_\odot$ binary the difference in going from 2PN to 3.5PN would be 22% and 60% (as opposed to 13% and 45% with 10^{-5} Hz) for chirp mass and η respectively. The number of GW cycles for a cut-off of 10^{-4} Hz is just 7 whereas with a 10^{-5} Hz cut-off it is as large as 540. Therefore, with a cut-off of 10^{-4} Hz, one is only observing the very late inspiral of the system[4] whereas with a cut-off of 10^{-5} Hz, the inspiral phase is dominant. The significantly larger variation in parameter estimation in going from 2PN to 3.5PN with the 10^{-4} Hz cut-off could be due to the generally accepted fact that higher order terms in the phasing formula are more important as one approaches the last stable orbit.

---

[4]Inspiral waveforms would be inadequate in this case. Theoretical approximants, e.g. Effective one body [48, 49] may have to be employed to model this phase of the binary's dynamics.

5.5 Parameter estimation without pattern averaging

Having discussed in detail the various aspects of parameter estimation using pattern averaged waveform and factors which affect the process, we now turn our attention to the parameter estimation without pattern averaging. Obviously the source's location, orientation and luminosity distance to the source gets added to the space of parameters which was four dimensional in the previous case. Unlike the ground based detectors, LISA can measure the distance, location and orientation of the source with a *single* detector because of the modulations due to its orbital motion [192, 193]. Besides, using LISA as a two detector network improves the estimation of angular resolution of the source [193]. In this section we will discuss the improvement brought in by the higher order terms using non-pattern averaged waveform for LISA. We check our code, which now includes the pattern functions, by reproducing the results of [193] at 1.5PN with their signal and noise models.

But as mentioned earlier, the strong dependence of the errors on the angular variables makes our analysis for selected values of angles (following Cutler [193]) non-generic. The best way to deal with this situation is to perform Monte Carlo simulations, similar to [198, 212, 21, 199]. However we notice that certain general conclusions can still be drawn from these specific cases and this will be the topic of discussion of the following section.

5.5.1 Comparison of different detector configurations

We compare the estimation of errors with different detector configurations now. The final errors, in comparison with the pattern averaged case, will depend on the following:

1. The value of SNR corresponding to the set of angles chosen

2. The change in SNR relative to the pattern averaged case and

3. The worsening of the errors due to the introduction of the new parameters.

For the pattern averaged case, since there are no pattern dependent parameters, the total parameter space is essentially 4 dimensional, the parameters being $\{t_c, \phi_c, \mathcal{M}, \eta\}$. When we make a transition from the pattern averaged to the non-pattern averaged case, five new parameters $\{D_L, \bar{\mu}_L, \bar{\mu}_S, \bar{\phi}_L, \bar{\phi}_S\}$ corresponding to the distance to the source, its location and orientation are added to the space of parameters. The parameter space is now nine dimensional significantly higher than the earlier four dimensional one. This increase in dimensionality of the parameter space leads to an increase in the errors of the four existing parameters. On the other hand, the introduction of pattern functions results in a change of SNR depending on the four angles chosen. The final picture is a complex interplay of all these features.
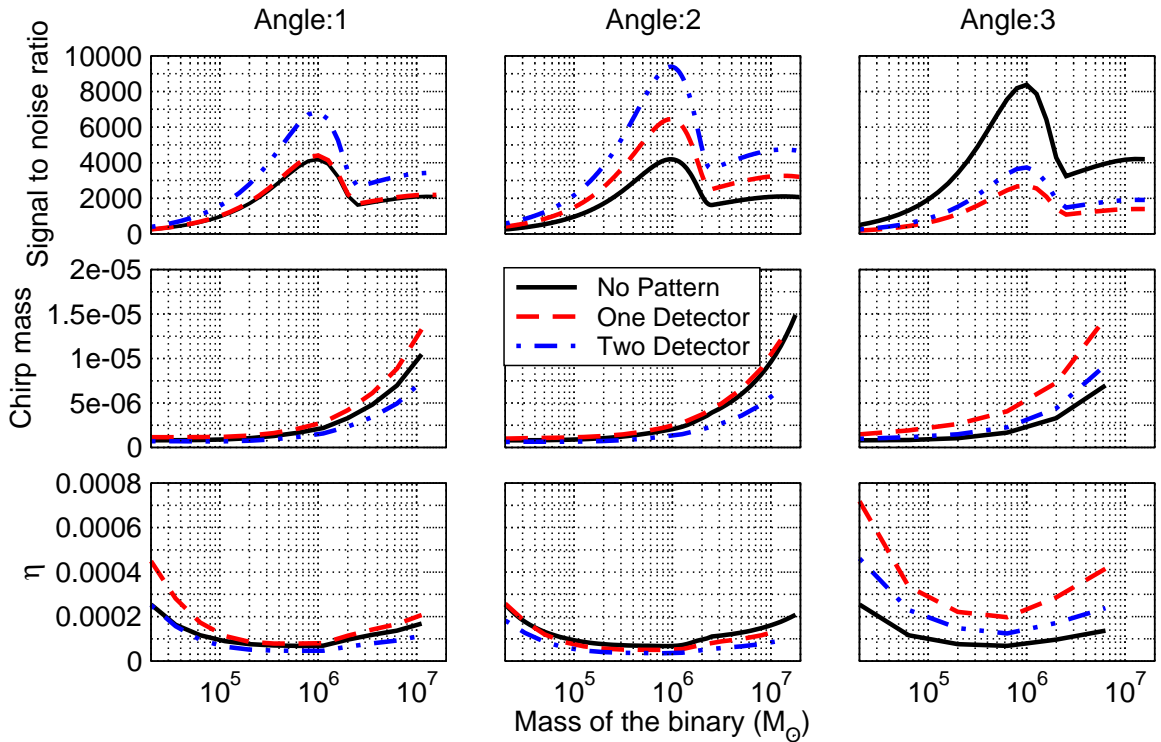
Figure 5.4: Variation of the signal to noise ratio, relative errors in chirp mass and relative errors in η with the total observed mass of the binary for different choices of location and orientation of the source. Sources are assumed to be at a luminosity distance of 3 Gpc and a *non-pattern averaged* waveform is used. Angle:1 corresponds to $\{\bar{\mu}_L = 0.5, \bar{\mu}_S = -0.8, \bar{\phi}_L = 3, \bar{\phi}_S = 1\}$. Angle:2 is $\{\bar{\mu}_L = 0.2, \bar{\mu}_S = -0.6, \bar{\phi}_L = 3, \bar{\phi}_S = 1\}$ and Angle:3 $\{\bar{\mu}_L = 0.8, \bar{\mu}_S = 0.3, \bar{\phi}_L = 2, \bar{\phi}_S = 5\}$. The errors thus depend very much on the position and orientation of the source in the sky.

The errors in chirp mass and η together with SNR is displayed in Fig. 5.4 for three set of angles from the seven given in [193]. The three configurations corresponding to the pattern averaged, non-pattern averaged with one detector and finally the two detector network (without pattern averaging) are considered. As is evident from the plot, the SNR and hence the errors crucially depend on the location and orientation of the source. Also, there can be orientations which may have a lower SNR than for the pattern averaged case (see third column e.g.). However an interesting conclusion from the figure (and from the runs corresponding to other values of angles which are not displayed) is that among the three effects which influence the parameter estimation without pattern averaging, the value of SNR seems to be the most dominant one. The smallest errors in the plot correspond to the configuration with the largest SNR. Between the pattern averaged and the one detector case, the effect of correlations due to the additional parameters play a significant role. For example, in the second column, though the one detector case has larger SNR, the errors

116

are smaller for the pattern averaged case for this reason. We do not discuss the percentage improvement arising from the higher order PN terms since it depends very much on the orientation of the source. Exhaustive Monte Carlo simulations have to be performed to have a detailed understanding of this.

We conclude with a remark about the estimation of angular resolution and distance as observed from the limited set of angles we have considered. The estimation of distance and angular resolution is not improved much because of the additional phasing terms. This is not surprising, since the additional terms in the phasing formula do not carry any information about location or orientation of the binary. One may need to go beyond the restricted waveform approximation in order to achieve this. Some preliminary studies in this regard [121, 122, 123, 124, 125, 126] are consistent with the same. Going beyond the restricted waveform approximation would mean including the amplitude corrections to the waveform from the two GW polarizations, currently completed up to 2.5PN order [101, 102]. This is because the amplitude terms are functions also of the angular positions of the source in the sky, the introduction of which could break different degeneracies, allowing better parameter estimation [123, 124].

5.6 Summary of results

The significance of higher order phasing terms is investigated in the LISA case for different sources using a *pattern averaged* waveform model. Using the 3.5PN inspiral waveform instead of the 2PN one which is currently employed in the GW experiments, mass parameters can be estimated with improved precision for LISA. Major conclusions of this study are as follows.

- For an equal mass binary of $2 \times 10^6 M_\odot$ at a luminosity distance of 3 Gpc, the improvement in chirp mass due to PN corrections in phasing formula beyond 2PN, is $\sim 11\%$ and that of η is $\sim 39\%$. For larger mass systems, the improvement is even more.

- Similar to the ground based detector case discussed in chapter 4, t_c shows trends opposite to that of the two mass parameters and estimation of it is worse by 43% for a $2 \times 10^6 M_\odot$ system.

- Most of the improvement (worsening) comes from the change from 2PN to 2.5PN transition after which the errors continue to oscillate, but with smaller amplitude indicating convergent behaviour beyond 2.5PN order.

- Correlation between the number of GW cycles is re-examined in the space based context. The number of GW cycles is a good indicator of how the errors vary with mass

but *not* across different PN orders.

- Parameter estimation for unequal mass binaries is also studied in the LISA context. The improvement in parameter estimation is more pronounced for binaries with unequal masses. For a binary consisting of an intermediate mass BH of $10^4 M_\odot$ and a SMBH of $10^6 M_\odot$, the improvements in chirp mass and η are 20% and 62% respectively. Our calculations do *not* apply to the extreme mass ratio case of, say, $10 M_\odot - 10^6 M_\odot$. This is because the Fisher matrix obtained in this case is very much ill-conditioned.

- The effect of the lower cut-off frequency we have chosen (10^{-5} Hz) on the parameter estimation is studied by comparing the calculation with the more modest cut-off of 10^{-4} Hz. Having a lower cut-off frequency 10^{-5} Hz, the parameter estimation improves very much for binaries whose masses are greater than $2 \times 10^{5.5} M_\odot$.

- The estimation of the luminosity distance to the source and its location and orientation is also studied using the non-pattern averaged waveform for selected source directions and orientations. They do *not* improve significantly by the use of the restricted 3.5PN template.

- Our analysis is based on a few systems with a few chosen orientations and hence cannot draw very general conclusions. However some general properties of the variation of errors with mass, using the non-pattern averaged waveform is discussed.

The very high accuracy parameter extraction possible with LISA will make it a useful tool of astrophysics and provide thorough probes of strong field aspects of gravity in the future.

5.7   Future directions

- **Monte Carlo simulations for the non-pattern averaged case:**
  Exhaustive Monte Carlo simulations are required in order to understand the effect of higher PN terms for LISA when the non-pattern averaged waveform is used since the parameter estimation in this case strongly depends on the location and orientation of the source. We plan to take up this problem in the near future.

- **Parameter estimation beyond the Fisher matrix:**
  It may be interesting to employ Markov chainMonte Carlo methods for parameter estimation [216, 215] and compare the results with the ones obtained using the covariance matrix. Extending this to the present context would surely be interesting and should be addressed.

- **Parameter estimation using the *full* waveform**:

  Our present study uses the restricted waveform approximation ignoring the presence of higher harmonics (beyond the leading quadrupolar frequency which is twice the orbital frequency) and neglects the amplitude corrections, in particular, to the leading harmonic from the higher PN order '+' and '×' polarizations. Recently Van den Broeck examined [125] the effect of inclusion of the above mentioned effects in the detection problem where he used the 2.5PN polarization [102] together with the 3.5PN phasing [99, 100]. He found that the restricted waveform significantly over-estimates the SNR. Parameter estimation with the full waveform in the LISA context may be an interesting problem to investigate since the amplitude terms contain additional information about the location and orientation of the binary and may improve, *e.g.*, the estimation of angular resolution of the source in the sky.

- **Effect of 2.5PN spin terms in parameter estimation**:

  Using the recent results for the 2.5PN phasing with spin-orbit coupling included [160, 119], one can investigate the effect of the inclusion of the 2.5PN spin terms. The analysis may be carried out both for the nonprecessing case (similar to [21]) and with simple precession (similar to [212]) and one can compare the results. Robustness of these results obtained using Cramer-Rao bound can be contrasted with a more rigorous bounds using Markov Chain Monte Carlo methods.

- **Including information about merger and ringdown**:

  Recently Luna and Sintes [191] examined the effect of including the ringdown information while performing the parameter estimation for compact binaries. They found significant improvement in error estimation when the total waveform was considered to be inspiral followed by ringdown in the case of LIGO and VIRGO. In the LISA context it may be interesting to do a similar exercise and study the results. One may also want to use the effective one-body (EOB) approach to model the late inspiral and the merger phase which will account for all the three phases of binary evolution. The correctness of using the EOB waveform to model merger may still be an open question.

- **Parameter estimation with TDI variables**:

  In the present analysis we have considered the noise of the two detectors to be uncorrelated. This is not true in reality. A more realistic analysis of the problem should involve and deal with the time delay interferometric variables [28].